

Individual characterization of fast-responding trap states at the NO-annealed SiO₂/4H–SiC interfaces

Takahiro Ono,¹ Mizuki Ohashi,² Tomohiro Shigeno,¹ Yutaro Uchida,¹ Yuuki Yasui,¹ Koji Kita,¹ and Yoshiaki Sugimoto^{1,*}

¹*Department of Advanced Materials Science, Graduate School of Frontier Sciences, The University of Tokyo, Kashiwa, Chiba, Japan*

²*Department of Applied Physics, Graduate School of Engineering, The University of Tokyo, Bunkyo, Tokyo, Japan*

(Dated: May 27, 2026)

Fast-responding trap states introduced by NO-annealing are suspected to limit the channel mobility of 4H–SiC MOSFETs, yet their microscopic characterization remains challenging because conventional electrical methods are spatially averaged and do not readily isolate such fast processes. Here, we visualize and analyze individual fast-responding trap states at the NO-annealed SiO₂/4H–SiC interface using the energy dissipation signal in frequency-modulation atomic force microscopy (FM–AFM), which selectively probes charge-exchange dynamics on sub- μ s time scales. Ring-shaped dissipation patterns were observed in the NO-annealed sample but not in the control sample without NO-annealing, indicating that the detected states are associated with nitridation. Spectroscopic measurements were also performed to determine the dependence of energy dissipation on the tip bias and the tip-sample distance. Combined with finite-element electrostatic calculations, this analysis allowed us to determine trap energies relative to the Fermi level, $E_t - E_F$, and revealed that the trap-energy distribution extends toward the interfacial conduction-band edge. These results provide microscopic evidence that NO-annealing generates fast-responding trap states near the SiO₂/4H–SiC interface.

I. INTRODUCTION

Wide-bandgap (WBG) semiconductors have attracted increasing attention as next-generation power-device materials, driven by the demand for higher efficiency and reliability in power conversion. Among WBG semiconductors, 4H–SiC is particularly promising because it combines a high critical breakdown electric field [1] with high thermal conductivity [2] and relatively weak anisotropy of electron mobility [3]. Moreover, a key processing advantage of SiC is that a high-quality SiO₂ gate dielectric can be readily formed by thermal oxidation, allowing metal–oxide–semiconductor (MOS) structures compatible with mature Si metal–oxide–semiconductor field-effect transistor (MOSFET) processing [4, 5].

Despite these advantages, the channel mobility in 4H–SiC MOSFETs is extremely low (≈ 5 cm²/Vs [6]) compared with the bulk electron mobility (1020–1200 cm²/Vs [3]). This degradation is generally attributed to a high density of electrically active defects remaining near the SiO₂/4H–SiC interface, including interface states and oxide-side near-interface traps. NO-annealing is commonly employed to improve the interface [7–10]; however, even NO-annealed devices typically exhibit channel mobilities of only ≈ 30 – 35 cm²/Vs (for the typical cases of $\sim 10^{16}$ cm⁻³ channel doping), which remain far below the values expected from bulk 4H–SiC [10].

Using high-frequency conductance analysis combined with theoretical modeling, Yoshioka *et al.* pointed out

the presence of fast-responding electrically active states associated with NO-annealing and further argued that interface-related traps with nanosecond-scale relaxation times, which are difficult to detect by conventional C – V measurements (typically up to ≈ 1 MHz), can degrade channel mobility [11, 12]. However, the microscopic origin of these fast-responding states and their quantitative impact on device performance remain under debate, in part because electrical measurements are spatially averaged and the separation of interface states and near-interface oxide traps can be model dependent [13, 14].

In this study, we spatially resolve and evaluate individual fast-responding trap states at the NO-annealed SiO₂/4H–SiC interface using the energy dissipation signal in frequency-modulation atomic force microscopy (FM–AFM). We can clearly discuss the in-plane distribution of individual traps assumed to exist at the interface. In this dissipation-based scheme, trap charging and discharging within an oscillation cycle of cantilever produce a hysteresis in the electrostatic force and an associated increase in the dissipated energy, providing selectivity to trap states with sub- μ s response times under our experimental conditions. Related dissipation-based approaches have previously been applied to isolated Au nanoparticles [15] and quantum dots [16]. Moreover, Cowie *et al.* recently reported the visualization of interface states at the SiO₂/Si interface using a dissipation-based method [17].

Figure 1 summarizes the trap-detection scheme based on the FM–AFM energy dissipation signal. Here, V_{tip} denotes the tip bias with respect to the sample and s the tip–sample distance. When a biased tip approaches the sample surface, the local electrostatic potential near

* ysugimoto@k.u-tokyo.ac.jp

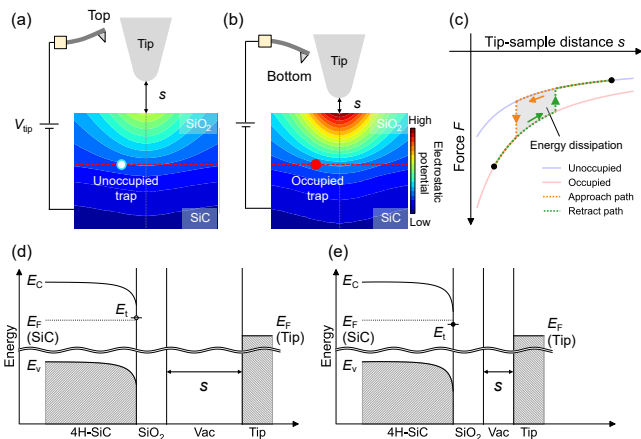


Figure 1. Schematic illustration of individual interface-trap detection by FM-AFM. (a) Electrostatic potential at the top of the tip oscillation cycle. (b) Electrostatic potential at the bottom of the cycle, where the higher potential induces trap occupation. (c) Schematic force-distance curve showing dissipation caused by hysteretic trap charging and discharging. (d) Band diagram of the SiC/SiO₂/vacuum/metallic-tip structure at positive tip bias with the tip farther from the surface. (e) Corresponding band diagram with the tip closer to the surface. Open and filled circles indicate unoccupied and occupied traps, respectively.

the interface is modified, which can switch the charge occupancy of a trap [Figs. 1(a) and (b)]. Figure 1(c) schematically illustrates the force-distance curve when the trap occupancy changes during an oscillation cycle of the tip. The electrostatic force acting on the tip of cantilever depends on the trap charge state. Because charge transfer at the trap involves a finite relaxation time, occupancy switching leads to different forces on the approach and retract paths, resulting in a hysteresis loop. This hysteresis loop increases the energy dissipation and is detected as the excitation-voltage signal in FM-AFM. At a given V_{tip} and s , the switching condition is satisfied at a constant lateral distance between tip and trap, thereby visualizing individual traps as ring-shaped dissipation patterns. Figures 1(d) and (e) show simulated band diagrams under positive tip bias. In this case, the SiC/SiO₂/vacuum/metallic-tip structure can be regarded as a MOS capacitor, in which the band bending near the interface is controlled by V_{tip} and s . As s decreases, the trap level E_t crosses the Fermi level E_F , resulting in a change in trap occupancy.

II. RESULTS AND DISCUSSION

We performed FM-AFM energy dissipation measurements on a SiO₂/4H-SiC(0001) sample in which nitrogen was introduced near the interface by direct NO-annealing of the 4H-SiC(0001) substrate [18]. Details of the sample preparation and FM-AFM measurements are given

in the Experimental Section. Figures 2(a) and (b) show dissipation images acquired at $V_{\text{tip}} = 4$ V and -2 V, respectively. The ring-shaped contrast is attributed to charge exchange at individual traps, and each ring center indicates the lateral trap position. In contrast, no rings were observed for a control SiO₂/4H-SiC(0001) sample in which an approximately 5-nm-thick oxide was formed by dry oxidation without NO-annealing (Supporting Information), indicating that the observed trap states are associated with the nitridation process. Since it is expected that NO treatment would reduce traps, this is an interesting observation.

Rings 1 and 2 in Fig. 2(a) have different radii, reflecting differences in trap energy. A smaller ring radius R implies that a larger effective electrostatic potential is required to bring the trap level across the Fermi level, whereas a larger R indicates that a smaller effective potential is sufficient. Figures 2(c)–(h) show two-dimensional dissipation maps measured while sweeping V_{tip} and s along the dashed lines in Figs. 2(a) and (b), which pass through the centers of the rings corresponding to individual trap positions. The parabolic bright ridges in these maps correspond to individual trap states, and the V_{tip} and s dependences of the ridge opening reflect the trap energy.

To quantify the trap energies, we calculated the electrostatic potential distribution using the finite element method and simultaneously fitted the calculated $R(V_{\text{tip}})$ and $R(s)$ curves to the experimental data (see Supporting Information for details). The electrostatic potential that simultaneously reproduces the observed V_{tip} and s dependences was identified with the energy offset between the trap level and the Fermi level in 4H-SiC, $E_t - E_F$. From this analysis, we obtained $E_t - E_F = 36$, 46, and -86 meV for rings 1–3, respectively.

To investigate the energy distribution of detectable trap states, we analyzed dissipation images acquired at different tip biases [Figs. 3(a)–(c)]. A custom deep-learning-based program automatically detected ring patterns and extracted the ring radius R [19, 20], yielding 95 rings at $V_{\text{tip}} = 4$ V [Fig. 3(a)] and 183 rings at $V_{\text{tip}} = -4$ V [Fig. 3(c)]. The extracted radii were then converted into trap-energy distributions using electrostatic potential simulations [Fig. 3(d)]. Figure 3(e) shows the resulting energy distribution of the interface trap density D_{it} for $V_{\text{tip}} = 4$ V and -4 V. The extracted D_{it} is on the order of 10^{10} – 10^{11} cm⁻²eV⁻¹, which is comparable to that of fast interface states reported for similar NO-annealed samples [11, 12]. Assuming that the interfacial band bending is laterally uniform in the absence of an external electric field, the energy distribution can also be expressed relative to the conduction-band edge at the interface, E_C . Here, E_C denotes the interfacial conduction-band edge after band bending rather than the bulk band edge. In this representation, D_{it} values are larger near E_C than in deeper energy regions. That is consistent with previous electrical studies [14, 21, 22] and indicates that the observed states are dominated by shallow acceptor-like electron trap states near the inter-

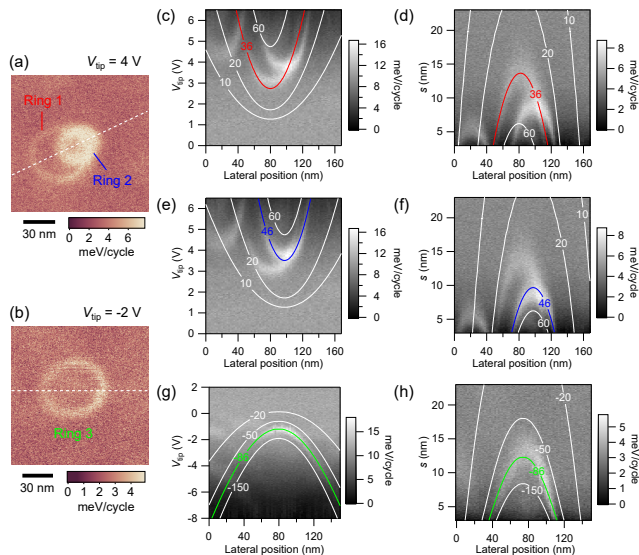


Figure 2. Energy dissipation imaging and dissipation spectroscopy of individual trap states at the NO-annealed $\text{SiO}_2/4\text{H-SiC}$ interface. (a) Dissipation image at $V_{\text{tip}} = 4$ V, showing rings 1 and 2. (b) Dissipation image at $V_{\text{tip}} = -2$ V, showing ring 3. (c-h) Two-dimensional dissipation maps measured along the dashed lines in (a) and (b) while sweeping V_{tip} or s : (c,d) ring 1, (e,f) ring 2, and (g,h) ring 3. Overlaid curves indicate equipotential contours calculated by the finite element method, and the labels give the energy relative to E_F in meV.

facial conduction-band edge.

We note that the reduced counts in the range $-250 < E_t - E_F < 50$ meV do not imply an intrinsic absence of trap states, but are most likely a methodological limitation. Because the dissipation contrast decays with increasing radius, trap states that respond only at very large ring radii under $V_{\text{tip}} = \pm 4$ V can produce signals too weak to exceed the detection threshold.

The ring patterns were observed only for the NO-annealed sample and were absent in the O_2 -annealed sample, indicating that the detected trap states are induced by nitridation. Because measurable dissipation requires charge switching of the trap within one oscillation cycle of the tip, the experimentally accessible relaxation time is estimated to be shorter than $1/(2f_0) = 1.8$ μs , where the cantilever's resonance frequency $f_0 = 284$ kHz. We could also observe the trap states in the cantilever's second resonance mode with $f = 1.76$ MHz (Supporting Information). These results indicate that the nitrogen-induced interface states respond well below 1 μs , consistent with previous reports [11, 12]. Our approach, which can analyze individual traps, does not rely heavily on modeling in contrast to the D_{it} estimation from device characteristics based on a modeling with presumed equivalent circuits. Therefore, we can confidently conclude that NO-annealing generates fast-responding trap states near the $\text{SiO}_2/4\text{H-SiC}$ interface. A plausible microscopic

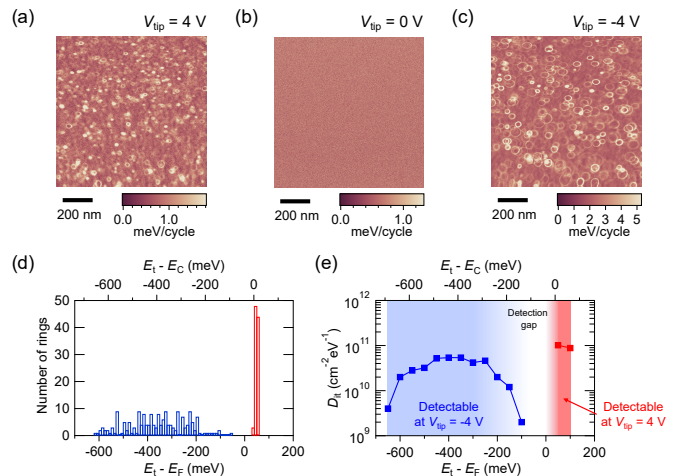


Figure 3. (a-c) Dissipation images acquired over a 1×1 μm^2 area at $V_{\text{tip}} = 4$ V, 0 V, and -4 V, respectively. (d) Ring-count distribution as a function of $E_t - E_F$ (bottom axis) and the corresponding $E_t - E_C$ values on the top axis, obtained from the detected ring radii using a bin width of 10 meV. Red and blue bins correspond to (a) and (c), respectively. (e) Energy distribution of D_{it} derived from (d). Red and blue shaded regions indicate the experimentally accessible energy windows at $V_{\text{tip}} = 4$ V and -4 V, respectively.

explanation is that nitrogen incorporated at the interface forms electrically active defects; one candidate is an NSi_3 -like configuration [23], although more complex nitrogen-related interfacial defects may also contribute. These results suggest that, although NO-annealing is widely used to improve the $\text{SiO}_2/4\text{H-SiC}$ interface, it can simultaneously generate fast-responding trap states near the conduction-band edge. These traps may affect the device's high-frequency operation.

III. CONCLUSION

In summary, we directly observed fast-responding trap states near the $\text{SiO}_2/4\text{H-SiC}$ interface using FM-AFM. Individual trap states were spatially separated and visualized as ring patterns in dissipation images. By comparing the dissipation maps with electrostatic potential simulations, we identified the energy levels of individual trap states in the nanoscale region. The presence of a high density of fast-responding trap states extending toward E_C suggests that NO-related defects provide electrically active states very close to the conduction-band edge. Our approach should be broadly applicable to the analysis of trap states in various power semiconductor and quantum-sensing devices.

IV. EXPERIMENTAL SECTION

A. Sample preparation

The sample structure was a 5-nm-thick SiO₂ layer on a 5- μ m-thick nitrogen-doped (*n*-type) 4H-SiC(0001) epitaxial layer with $N_D \approx 1 \times 10^{16} \text{ cm}^{-3}$. After HF cleaning, the sample was directly annealed at 1150°C for 120 min in an NO/N₂ ambient (NO/N₂ = 1/2) to form a SiO₂ layer with nitrogen incorporated mostly near the interface [18]. The nitrogen content in the bulk part of the film was confirmed to be only 1 at.%. After loading the sample into the vacuum chamber, FM–AFM measurements were performed without any degassing.

B. FM–AFM measurements

All AFM measurements were performed at room temperature in an ultrahigh-vacuum chamber ($\sim 10^{-11}$ Torr) using a custom-built AFM based on optical interferometry and operated in the frequency-modulation (FM)

mode. In this mode, the energy dissipation was evaluated from the excitation voltage required to maintain a constant cantilever oscillation amplitude.

Commercial Pt-coated Si cantilevers were used as force sensors. The cantilevers had a resonance frequency of $f_0 = 284 \text{ kHz}$, a spring constant of $k = 19 \text{ N/m}$, and a quality factor of approximately 2×10^4 . Before the measurements, the cantilevers were cleaned by Ar⁺ ion sputtering (0.6 keV, 3×10^{-7} Torr, 25 min). This sputter-cleaning process removes the native oxide and other contaminants from the tip apex, thereby maintaining good tip conductivity during the measurements. The oscillation amplitude was set to $A = 500 \text{ pm}$.

ACKNOWLEDGMENTS

This work was supported by JST SPRING Grant No. JPMJSP2108, JST FOREST Program Grant No. JPMJFR203J, and JSPS KAKENHI Grant Nos. 25K22215, 26K01386, 26H01330, and 24H00308. Y. S. acknowledges support from the Precise Measurement Technology Promotion Foundation (PMTF-F) and the Iwatani Naoji Foundation.

-
- [1] P. Godignon, J. Biscarrat, M. Tranchesset, R. Lavieville, D. Tournier, P. Brosselard, and J. Montserrat, Breakdown voltage capability of vertical 4H–SiC power devices, *Mater. Sci. Semicond. Process.* **178**, 108347 (2024).
- [2] X. Qian, P. Jiang, and R. Yang, Anisotropic thermal conductivity of 4H and 6H silicon carbide measured using time-domain thermoreflectance, *Mater. Today Phys.* **3**, 70 (2017).
- [3] T. Kimoto and J. A. Cooper, *Fundamentals of Silicon Carbide Technology: Growth, Characterization, Devices, and Applications*, 1st ed. (John Wiley & Sons, 2014).
- [4] S. Li, J. Luo, and T. Ye, Investigation of Reducing Interface State Density in 4H-SiC by Increasing Oxidation Rate, *Nanomaterials* **13**, 1568 (2023).
- [5] M. Green, E. Gusev, R. Degraeve, and E. Garfunkel, Ultrathin (<4 nm) SiO₂ and Si-O-N Gate Dielectric Layers for Silicon Microelectronics: Understanding the Processing, Structure, and Physical and Electrical Limits, *J. Appl. Phys.* **90**, 10.1063/1.1385803 (2001).
- [6] H. Yano, T. Hirao, T. Kimoto, and H. Matsunami, High Channel Mobility in Inversion Layer of SiC MOSFETs for Power Switching Transistors, *Jpn. J. Appl. Phys.* **39**, 2008 (2000).
- [7] A. M. Vidarsson, D. Haasman, S. Dimitrijević, and E. Ö. Sveinbjörnsson, Improvement of channel-carrier mobility in 4H-SiC MOSFETs correlated with passivation of very fast interface traps using sodium enhanced oxidation, *AIP Adv.* **13**, 055126 (2023).
- [8] T.-H. Kil and K. Kita, Anomalous band alignment change of SiO₂/4H-SiC(0001) and (000-1) MOS capacitors induced by NO-POA and its possible origin, *Appl. Phys. Lett.* **116**, 122103 (2020).
- [9] J. Rozen, S. Dhar, S. K. Dixit, V. V. Afanas'ev, F. O. Roberts, H. L. Dang, S. Wang, S. T. Pantelides, J. R. Williams, and L. C. Feldman, Increase in oxide hole trap density associated with nitrogen incorporation at the SiO₂/SiC interface, *J. Appl. Phys.* **103**, 124513 (2008).
- [10] G. Chung, C. Tin, J. Williams, K. McDonald, R. Chanana, R. Weller, S. Pantelides, L. Feldman, O. Holland, M. Das, and J. Palmour, Improved inversion channel mobility for 4H-SiC MOSFETs following high temperature anneals in nitric oxide, *IEEE Electron Device Lett.* **22**, 176 (2001).
- [11] H. Yoshioka, T. Nakamura, and T. Kimoto, Generation of very fast states by nitridation of the SiO₂/SiC interface, *J. Appl. Phys.* **112**, 024520 (2012).
- [12] H. Yoshioka, T. Nakamura, and T. Kimoto, Characterization of very fast states in the vicinity of the conduction band edge at the SiO₂/SiC interface by low temperature conductance measurements, *J. Appl. Phys.* **115**, 014502 (2014).
- [13] Y.-X. Wen, B.-Y. Tsui, and K. P. Cheung, Impact of near interface defects on NO annealed SiC MOSFET mobility, *Microelectron. Reliab.* **173**, 115841 (2025).
- [14] W. Huang, P. Dong, N. Yang, Y. Ma, Q. Xu, C. Fu, M. Huang, Y. Li, Z. Yang, M. Gong, D. He, and Q. He, Effects of nitrogen passivation on the capture cross section energy distribution of 4H-SiC/SiO₂ interface defects and the temperature dependences of leakage current, *Appl. Phys. Lett.* **127**, 122101 (2025).
- [15] A. Tekiel, Y. Miyahara, J. M. Toppo, and P. Grutter, Room-Temperature Single-Electron Charging Detected by Electrostatic Force Microscopy, *ACS Nano* **7**, 4683 (2013).
- [16] Y. Miyahara, A. Roy-Gobeil, and P. Grutter, Quantum state readout of individual quantum dots by electrostatic

- force detection, *Nanotechnology* **28**, 064001 (2017).
- [17] M. Cowie, T. J. Z. Stock, P. C. Constantinou, N. J. Curson, and P. Grütter, Spatially Resolved Dielectric Loss at the Si/SiO₂ Interface, *Phys. Rev. Lett.* **132**, 256202 (2024).
- [18] Y. Uchida, A. Tamura, and K. Kita, Study on direct NO oxynitridation of 4H-SiC (0001): time dependent change in SiC surface reaction rate and electrical characteristics of SiO(N)/SiC interface, *Jpn. J. Appl. Phys.*, in press (2026).
- [19] A. J. Czarnecki, N. L. Kolev, P. See, N. J. Sullivan, W. A. Behn, N. J. Curson, T. J. Z. Stock, and P. Grütter, Hydrogen passivation effects on spatially resolved charge trap densities in Si(100)-SiO₂, *AIP Adv.* **15**, 105024 (2025).
- [20] A. Paszke, S. Gross, F. Massa, A. Lerer, J. Bradbury, G. Chanan, T. Killeen, Z. Lin, N. Gimelshein, L. Antiga, A. Desmaison, A. Kopf, E. Yang, Z. DeVito, M. Raison, A. Tejani, S. Chilamkurthy, B. Steiner, L. Fang, J. Bai, and S. Chintala, PyTorch: An Imperative Style, High-Performance Deep Learning Library, in *Advances in Neural Information Processing Systems 32*, edited by H. Wallach, H. Larochelle, A. Beygelzimer, F. d. Alché-Buc, E. Fox, and R. Garnett (Curran Associates, Inc., 2019) pp. 8024–8035.
- [21] D. Zhai, D. Gao, J. Xiao, X. Gong, J. Yang, Y. Zhao, J. Wang, and J. Lu, Electrical characterization of near-interface traps in thermally oxidized and NO-annealed SiO₂/4H-SiC metal-oxide-semiconductor capacitors, *J. Phys. D: Appl. Phys.* **53**, 445102 (2020).
- [22] P. Fiorenza, M. Zignale, M. Camalleri, L. Scalia, E. Zanetti, M. Saggio, F. Giannazzo, and F. Roccaforte, Impact of the NO annealing duration on the SiO₂/4H-SiC interface properties in lateral MOSFETs: The energetic profile of the near-interface-oxide traps, *Materials Science in Semiconductor Processing* **169**, 107866 (2024).
- [23] Y. Xu, X. Zhu, H. D. Lee, C. Xu, S. M. Shubeita, A. C. Ahyi, Y. Sharma, J. R. Williams, W. Lu, S. Ceesay, B. R. Tuttle, A. Wan, S. T. Pantelides, T. Gustafsson, E. L. Garfunkel, and L. C. Feldman, Atomic state and characterization of nitrogen at the SiC/SiO₂ interface, *J. Appl. Phys.* **115**, 033502 (2014).